Apparent Decreases in Colloid Deposition Rate Coefficients with Distance of Transport under Unfavorable Deposition Conditions: A General Phenomenon

XIQING LI,[†] TIMOTHY D. SCHEIBE,[‡] AND WILLIAM P. JOHNSON*,[†]

Department of Geology & Geophysics, University of Utah, Salt Lake City, Utah, and Pacific Northwest National Laboratory, Richland, Washington

The transport of polystyrene microspheres was examined in packed glass beads under a variety of environmentally relevant ionic strength and flow conditions. The observed profiles of numbers of retained microspheres versus distance from the column entrance were much steeper than expected based on a constant rate coefficient of deposition across the length of the column, indicating apparent decreases in deposition rate coefficients with transport distance. Deviation in the profile from log-linear decreases with distance was greatest under highly unfavorable conditions (low ionic strength), relatively reduced under mildly unfavorable conditions (high ionic strength), and was eliminated under favorable conditions. The generality of apparent decreases in deposition rate coefficients with distance of transport among microspheres, bacteria, and viruses leads to the conclusion that such effects reflect processes that are fundamental to filtration under unfavorable conditions. Numerical simulations of experiments that were performed under unfavorable conditions utilized a log-normal distribution of deposition rate coefficients among the colloid population in order to simulate the effluent curves and retained profiles simultaneously. It is shown that while straining could be a significant contributor to the steep retained profiles at low ionic strength, where overall retention is low, distribution in interaction potentials among the population was a viable mechanism that can yield apparent decreases in deposition rate coefficients with distance of transport.

Introduction

The observation that rate coefficients of colloid deposition are not constant with transport distance was first recognized in the bacterial transport literature (*1*). Concentrations of retained cells decreased faster with distance of transport than would have been expected based on a constant first order rate coefficient of deposition across the packed porous media column. A decreasing deposition rate coefficient with transport distance was required in order to simulate the profile of retained cells. In contrast, the dominant theory for colloid transport in porous media assumes a spatially constant deposition rate coefficient (*2*), which yields a log-linear decrease in retained and mobile particle concentrations with distance of transport. Apparent changes in deposition rate coefficients with distance now appear to be the norm rather than the exception in the transport of bacteria in the laboratory (*1*, *3*−*6*) and bacteria in the field (*7*−*9*) as well as viruses in the laboratory (*10*, *11*) and the field (*12*−*15*).

Spatial decreases in deposition rate coefficient in the field can in some cases be attributed to heterogeneity in the porous media (e.g. grain size and surface charge) (e.g. ref *14*). However, porous media heterogeneity cannot explain the observed steep distributions of retained cells in column experiments, since properties should be evenly distributed across a system of packed porous media. Spatial decreases in deposition rate coefficients have been tentatively attributed to distributions in surface properties among the particle population, resulting in up-gradient deposition of those bacteria having higher deposition rate coefficients relative to the other bacteria in the population. The observation indicates that the cell population should become less sticky with increasing distance of transport. To explain the retained profile, the distribution of deposition rate coefficients among the cell population must typically be wide, e.g. described by a log-normal distribution or a power law (*10*, *11*, *16*). This distribution can be considered to derive from a distribution in cell-grain interaction potentials among the cell population.

In contrast, the literature concerning nonbiological colloid transport has only recently explored the existence of distributed deposition rate coefficients, possibly because examinations of experimentally determined profiles of retained colloids with distance of transport are nearly absent from this literature. Distributions in deposition rate coefficients (distributions in interaction potentials) have been considered as a possible cause of the observed weak dependence of deposition efficiencies on salt concentrations relative to what would be expected from theory (*17*). However, relatively narrow deposition rate coefficient distributions were considered (10% c.v. for normal distribution), and this may be why they were not sufficient to explain the observations.

In contrast to the literature concerning colloid deposition, the literature concerning *re-entrainment* of nonbiological colloids from porous media recognizes the existence of wide distributions of re-entrainment rate coefficients (log-normal or power law) among the retained population (*18*−*22*). Distributions in deposition rate coefficients (as determined from the apparent decrease in deposition rate coefficients with distance of transport) can be attributed to only a subset of the potential factors that can be expected to yield distributed *re-entrainment* rate coefficients, since the latter can include effects from sediment surface charge heterogeneity and roughness.

Very recently, Bradford et al. (*23*) showed that carboxylated latex microspheres of different sizes displayed steeper decrease of retained profiles (in glass beads and quartz sand) relative to what would be expected from a constant rate of deposition. The authors hypothesized that physical straining caused enhanced deposition at the influent end of the column on the basis that deposition was favored by larger particle diameters and smaller collector diameters.

The objective of this paper is to describe a series of experiments examining the transport of carboxylated latex microspheres in glass beads under various flow and ionic strength conditions. The intent of the experiments was to examine trends in the simulated deposition and re-entrainment parameters and their relationship to interaction forces

* Corresponding author phone: (801)581-5033; fax: (801)581-7065; e-mail: wjohnson@mines.utah.edu.

[†] University of Utah.

[‡] Pacific Northwest National Laboratory.

10.1021/es049154v CCC: $27.50
Published on Web 00/00/0000

and hydrodynamic drag. However, the retained profiles were not consistent with a constant first order deposition rate coefficient across the column; rather, they indicated a decreasing rate coefficient of colloid deposition with increasing transport distance. It is the purpose of the present paper to discuss the significance of the retained profiles of nonbiological colloids. It is proposed that the apparent decrease in colloid deposition rate coefficients with distance of transport is ubiquitous in the transport of biological and nonbiological colloids and that the observation reflects contributing processes that are fundamental to filtration. The sensitivity of the retained profiles to ionic strength and flow rate precludes colloid straining (at least as a purely physical process) as a sole contributing mechanism. Other potential contributing mechanisms evaluated include distributed interaction potentials (log-normal) among the colloid population and depletion of colloids from the perimeter of the pore space (water adjacent to sediment grain surfaces) during transport. It is shown that pore-perimeter depletion is not consistent with the experimental results.

Methods

Experimental Conditions. The microspheres used in column experiments were spherical fluorescent carboxylate-modified polystyrene latex microspheres of two similar sizes but different surface charge densities (1.1 and 1.0 μm diameter, surface charge density 0.18 meq-g^{-1} and 0.015 meq-g^{-1}, respectively). The microsphere stock suspensions (Molecular Probes, Inc., Eugene, OR) were used as received with a particle concentration of 2.7×10^{10} mL^{-1} (1.1 μm) and of 3.6×10^{10} mL^{-1}(1.0 μm). Both stock suspensions contain 2 mM of NaN_3 as antibacterial agent. Prior to injection, an aliquot of stock suspensions was diluted to achieve an influent concentration (C_o) of 3.5×10^6 ±15% particles-mL^{-1} in salt solution with the desired ionic strength. The minor variation in influent concentration was most likely caused by intake fluctuation of the micropipet during dilution in each experiment.

Spherical soda lime glass beads (Cataphote Inc., Jackson, MS) were used as the porous media. The glass beads were dry-sieved using 30 and 40 mesh U.S.A. standard testing sieves (The W.S Tyler Company, Mentor, Ohio), resulting in glass bead sizes ranging from 417 and 600 μm. The glass beads were first rinsed sequentially with acetone and hexane and then soaked with concentrated HCl for about 24 h, followed by repeated rinsing with ultrapure water (Millipore Corp. Bedford, MA) until the ionic strength was negligible relative to the experimental ionic strength, as determined using a conductivity meter (Conductance/TDS Model 72, Engineered Systems & Design, Newark, DE).

The cylindrical Plexiglass columns (20 cm in length and 3.81 cm in inner diameter) were dry-packed after the glass beads were dried at 105 °C and cooled. Packing was performed by adding glass beads in small increments (~2 cm) with mild vibration of the column. Two 60-mesh stainless steel screens (Gerard Daniel Worldwide, Hanover, PA) were placed at each end of the column. To spread the flow upon entry into the column, 3.5 g of same glass beads was added to the top of the influent screen, forming a 2 mm-thick layer that was covered by another screen. The mass of packed glass beads in each column differs by no more than 2 g. The porosity of the packed glass beads was 0.373, as determined by weighing before and after saturating the column and dividing aqueous phase volume derived from the mass difference by the total volume of the column.

The packed columns were purged with CO_2 for at least 15 min to replace air (since CO_2 is soluble in water) and were then flushed with HCl solution at pH 3.0 for 24 h at an average flow rate of 2.8 mL-min^{-1}. This flushing with pH 3.0 solution was intended to dissolve Na_2O and CaO at the glass bead surface and allow subsequent pH equilibration (*24*). After flushing, the columns were preequilibrated for about 10 pore volumes with microsphere-free salt solution at pH of 6.92, buffered by MOPS/NaOH. One pore volume was equal to 84.5 mL at a porosity of 0.373.

Following preequilibration, the effluent pH was found to consistently differ by no more than 0.02 units from that of the influent. The buffered solutions were prepared by adding 0.46 g/L of MOPS and 0.04 g/L NaOH and adjusting with NaCl to achieve desired ionic strengths. The contribution to the ionic strength from the buffer is 0.001 M; therefore, no NaCl was added for solution at this ionic strength. Organic buffer MOPS was used because preequilibration with salt solution buffered with $NaHCO_3$ resulted in slow increase of pH by over 1 unit within 24 h. Such slow increase was not reported in previous studies (e.g. refs *24* and *25*), presumably because their flow rates were much higher than the ones examined here and their experiment durations were much shorter. Slow increase in pH indicates continual dissolution of Na_2O, CaO, and perhaps other metal oxides. For this reason, the metal ion concentrations of influent and effluent were analyzed using Inductively Coupled Plasma Atomic Emission Spectroscopy (ICP-AES, Perkin-Elmer Inc., Boston, MA) during one experiment to qualitatively determine the magnitude of possible increases.

After preequilibration, 3 pore volumes of microsphere suspension were injected, followed by elution for 7 pore volumes with buffered salt solution (without microspheres) at the same ionic strength and pH. During injection, the microsphere suspension reservoirs were sonicated for 1 min each hour to minimize aggregation, as verified by flow cytometric analyses. For the high surface charge carboxylated microspheres (1.1 μm), the transport experiments were carried out at three ionic strengths, 0.006, 0.02, and 0.05 M. The flow rate was varied to produce pore water velocities at 2, 4, and 8 m-day^{-1}. For the low surface charge carboxylated microspheres (1.0 μm), transport experiments were conducted at one ionic strength (0.02 M) and one flow rate (8 m-day^{-1}). The experimental conditions are summarized in Table 1.

The suspensions and solutions were injected in up-flow mode using a syringe pump (Harvard Apparatus, Inc, Holliston, MA). During injection the syringes were refilled every 23 mL (about every 40, 20, and 10 min, respectively,

TABLE 1. Column Experiment Conditions, Mass Balances, and Model Parameters for Simulations Using the Particle-Tracking Model[a]

size (μm)	IS (M)	Vel	N	% Rec	% Sed	k_f (h^{-1})	k_r (h^{-1})	f_{ir}	$\sigma_{\ln kf}$
1.1	0.006	4	2	100.0	2.4	0.024[b]	0.23[b]	0.85[b]	0
1.1	0.02	4	2	106.5	25.4	0.23[b]	0.18[b]	0.967[b]	0
1.1	0.05	4	2	94.4	55.0	0.74[b]	0.14[b]	0.992[b]	0
1.1	0.006	4	2	100.0	2.4	0.28	0.23	0.73	5.3
1.1	0.02	4	2	106.5	25.4	0.84	0.18	0.945	2.2
1.1	0.05	4	2	94.4	55.0	3.64	0.14	0.982	1.8
1.1	0.02	2	2	88.8	45.5	0.31[b]	0.04[b]	0.983[b]	0
1.1	0.02	8	2	101.1	8.7	0.16[b]	0.42[b]	0.971[b]	0
1.1	0.02	2	2	88.8	45.5	16.6	0.03	0.91	4.5
1.1	0.02	8	2	101.1	8.7	0.39	0.4	0.96	2.3
1.0	0.02	8	2	93.5	20.0	0.58[b]	0.15[b]	0.4[b]	0
1.0	0.02	8	2	93.5	20.0	5.3	0.2	0.012	3.2
0.93	0.001	4[c]	1	101.8	100.7	4.0[b]	0.1[b]	0.996[b]	0
0.93	0.001	8[c]	2	97.6	92.9	5.0[b]	0.1[b]	0.992[b]	0

[a] "Size" refers to diameter of microspheres. "IS" indicates ionic strength (M), "Vel" indicates pore water velocity (m-day^{-1}). "N" refers to the number of replicates. "% Rec" refers to average percent recovery for the experimental condition. "% Sed" refers to average percent of microspheres retained on sediment at end of the experiment. [b] Refers to parameter values determined with single k_f (std. dev.lnk_f, $\sigma_{\ln kf} = 0$), where $\sigma_{\ln kf} \neq 0$, k_f refers to mean of log-normal distribution. [c] Refers to experiments for which model with single k_f can fit both the effluent curves and retained profiles simultaneously.

at flow rates of 2, 4, and 8 m-day^{-1}). The refill rate was set at 50 mL-min^{-1} for flow rates at 2 and 4 m-day^{-1}, and at 60 mL-min^{-1} for flow rate at 8 m-day^{-1}, resulting in flow interruption of 1.5, 1.0, and 0.65 min, respectively, at these three flow rates. During the switch from injection to elution, flow was interrupted for 3−6 min when syringes and tubing were rinsed with microsphere-free solutions. For some experiments at 4 m-day^{-1}, flow interruption was minimized by using a push−pull setup in which one syringe injected, while the other one refilled. However, this approach was abandoned since the decrease in flow interruption associated with refilling was balanced by increases in flow interruption associated with switching from injection to elution (more syringes needed to be rinsed). Flow interruptions seemed to have had no noticeable effects on microsphere deposition and re-entrainment dynamics, as indicated by the continuity of the breakthrough-elution curves (shown below).

Column effluent samples were collected in 5 mL polystyrene tubes using a fraction collector (CF-1, Spectrum Chromatography, Houston, TX). Following the experiment, the sediment was dissected into 10 2 cm-long segments, as the sediment was released from the column under gravity. Retained colloids were recovered by placing sediment segments (2 cm) into specified volumes of Milli-Q water and sonicating for 1 min, followed by manual vigorous shaking for a few seconds. These specified volumes were 100 mL, for the first three segments at the column inlet, and 25 mL for all subsequent segments.

Aqueous effluent samples, and supernatant samples from recovery of retained microspheres, were analyzed using flow cytometry (BD FACScan, Becton Dickinson & Co., Franklin Lakes, NJ). The samples were run using a flow rate of 12 μL-min^{-1} at an excitation wavelength of 488 nm and were counted for 1 min. Conversion of "event" counts on the flow cytometer into microsphere concentrations was made using a calibration curve based on serial dilutions of microsphere suspensions of known concentration. The R^2 of the log−log calibration curves were consistently greater than 0.99. The flow cytometer was able to track aggregation of microspheres as doublets and triplets based on their respective light scattering properties.

The area under the breakthrough-elution curve was integrated to yield the percentage of microspheres exiting the column. The percent of injected microspheres recovered from the sediment was determined by summing the number of microspheres recovered from all segments of the sediment and dividing by the total number injected. The overall recovery (mass balance) of microspheres was determined by summing the percentages of microspheres that exited and that were retained in the column.

Numerical Simulations. A one-dimensional discrete random-walk particle-tracking model (developed at PNNL) was used to simulate colloid transport in the column experiments. The model has been previously applied to simulate bacterial transport with emphasis on characterization of long-term detachment and tailing (*9*) and size exclusion (*26*). The model treats advection and dispersion using conventional random-walk particle methods as described in Scheibe and Wood (*26*). Deposition is governed by a relationship of the form

$$\frac{\partial C}{\partial t} = -k_f C \tag{1}$$

where C is the concentration of suspended colloids (number per unit fluid volume) and k_f is the deposition rate coefficient. In the case where k_f is assumed to be a single constant under prescribed flow conditions, as is common in microbial and colloid transport modeling, this continuum form can be easily solved and codes are widely available (e.g., CXTFIT, (*27*)). However, a particle-based formulation is more readily applied to problems in which more complex representations of deposition rate coefficients are used, such as random distributions of rate coefficients as considered here. In the particle model, eq 1 is represented in a discrete form by assigning a probability of deposition to each numerical particle in each time step. The probability of deposition in any time step is given by the deposition rate coefficient multiplied by the time step. An analogous procedure is used to represent the re-entrainment process using a re-entrainment rate coefficient (k_r) that is applied to the reversibly deposited population of colloids. The particle model also allows for the simulation of partially irreversible deposition via a fraction of irreversible deposition (f_{ir}) that is specified by the user. At each time step and for each numerical particle, a uniform pseudorandom number between 0 and 1 is generated and compared to the probability of deposition (or re-entrainment). If the random numbers is less than the assigned probability, then deposition (or re-entrainment) occurs. Likewise, a uniform pseudorandom number is generated upon occurrence of deposition and compared to f_{ir}. If the random number is less than f_{ir}, then the particle is assigned a flag that designates it as irreversibly deposited, and it will not be subsequently considered for re-entrainment.

Representation of a distribution of deposition rate coefficients among a population of colloids is straightforward. Each numerical particle is treated by the code as an object with attributes, one of which can be a particle-specific deposition rate coefficient. The deposition rate coefficients associated with each particle are determined upon initiation of the code by generating pseudorandom numbers from the prescribed distribution. To eliminate the possibility of negative deposition rate coefficient, we utilize a log-normal distribution parametrized by its mean and standard deviation (although other distributions are certainly plausible, e.g. ref *16*). The mean deposition rate coefficient (μ_{k_f}) and the standard deviation of the natural logarithm of the deposition rate coefficient ($\sigma_{\ln k_f}$) are specified by the user. The mean and variance of k_f are given by (e.g., ref *28*)

$$\mu_{k_f} = \theta_{k_f} e^{-(\sigma^2_{\ln k_f}/2)} \tag{2a}$$

$$\sigma_{k_f}^2 = \mu_{k_f}^2(\exp(\sigma^2_{ln\ k_f}) - 1) \tag{2b}$$

where θ is the median of the distribution. Note that $\ln\theta_{k_f} = \theta_{\ln k_f}$ because the natural log transformation is monotonic and that $\theta_{\ln k_f} = \mu_{\ln k_f}$ because the normal distribution is symmetric. It follows that $\mu_{\ln k_f} = \ln\theta_{k_f}$. Taking the natural logarithm of both sides of eq 2a, substituting this relationship, and rearranging yields

$$\mu_{\ln k_f} = \ln(\mu_{k_f}) + (\sigma_{\ln k_f}^2/2) \tag{3}$$

Given the input values and eq 3, the mean and standard deviation of $\ln k_f$ are determined. The RNNOF function from the IMSL Statistical Libraries (Digital Fortran, Compaq, Inc.) is used to generate a standard normal pseudorandom number γ_i with mean 0 and standard deviation 1 for each particle (i = 1 to N_p. N_p is the number of particles) that is then scaled and back-transformed to obtain a unique deposition rate coefficient associated with each particle:

$$k_{f_i} = \exp(\gamma_i \sigma_{\ln k_f} + \mu_{\ln k_f}) \tag{4}$$

Results

Mass Balances. Mass recoveries (total from effluent and sediment) were virtually all between 89% and 107%, with the vast majority showing between 95% and 105% recovery (Table

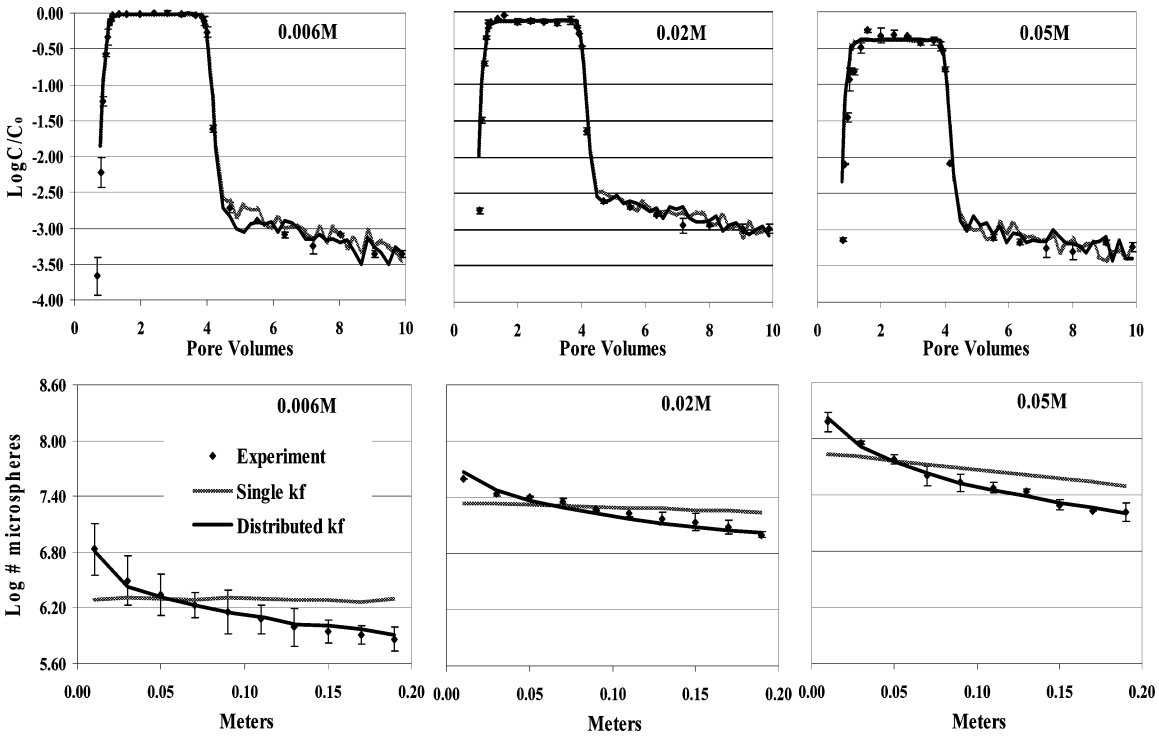

FIGURE 1. Ionic strength series for 1.1-μm microspheres at flow rate = 4 m-day^{-1}, showing effluent breakthrough-elution curves (top) and retained profiles (bottom). Error bars represent standard deviations in results from replicate experiments (n = 2). Simulations using the particle transport model with a single deposition rate coefficient (single k_f, dashed line) are contrasted against those using a deposition rate coefficient distribution (distributed k_f, solid line).

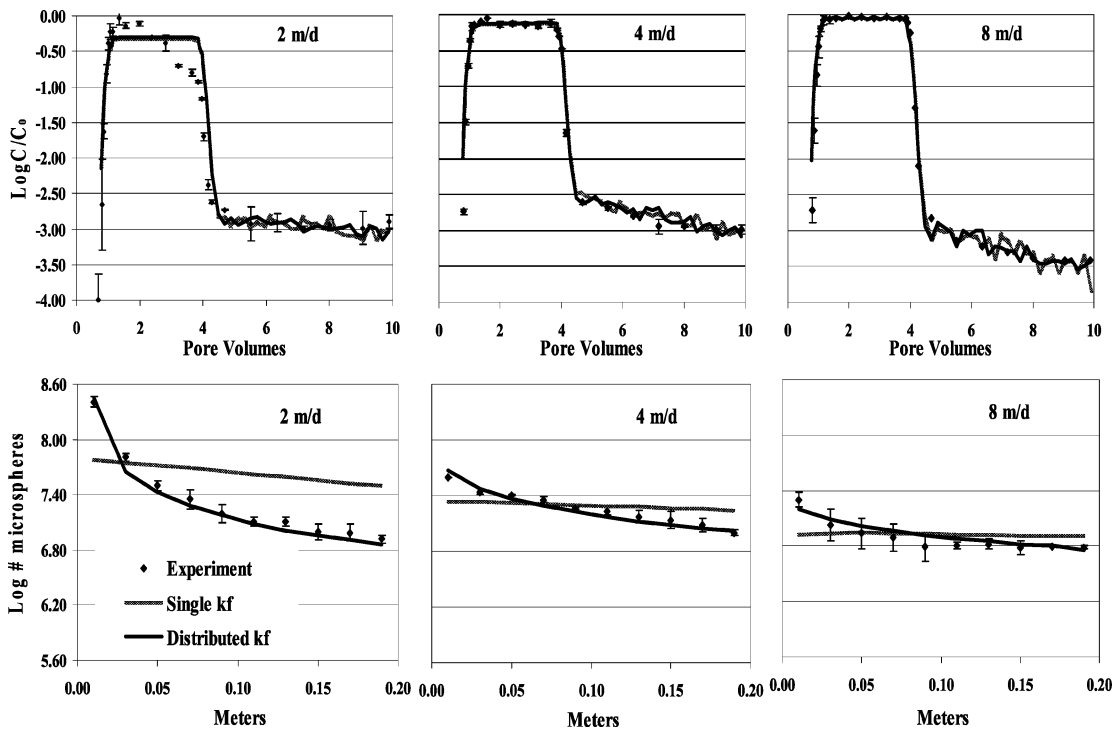

FIGURE 2. Flow rate series at ionic strength = 0.02 M, for 1.1-μm microspheres, showing effluent breakthrough-elution curves (top) and attached profiles (bottom). Simulations are shown using the particle transport model with and without k_f distribution (solid and dashed line, respectively). As well, one simulation (dashed line) shows the inability to simultaneously fit both the retained profiles and the effluent curves.

1). The excellent mass balance shows that the microspheres were detached by dilution into pure water, indicating that their mechanism of deposition was eliminated either by disassembling the pore structure or by increasing the magnitude of colloid-collector electrostatic repulsion.

The effluent breakthrough-elution curves for the 1.1-μm microspheres at different ionic strengths and flow rates are shown in Figures 1 and 2, respectively. Error bars in the effluent breakthrough-elution curves and the retained profiles (Figures 1−3) represent standard deviations from replicate

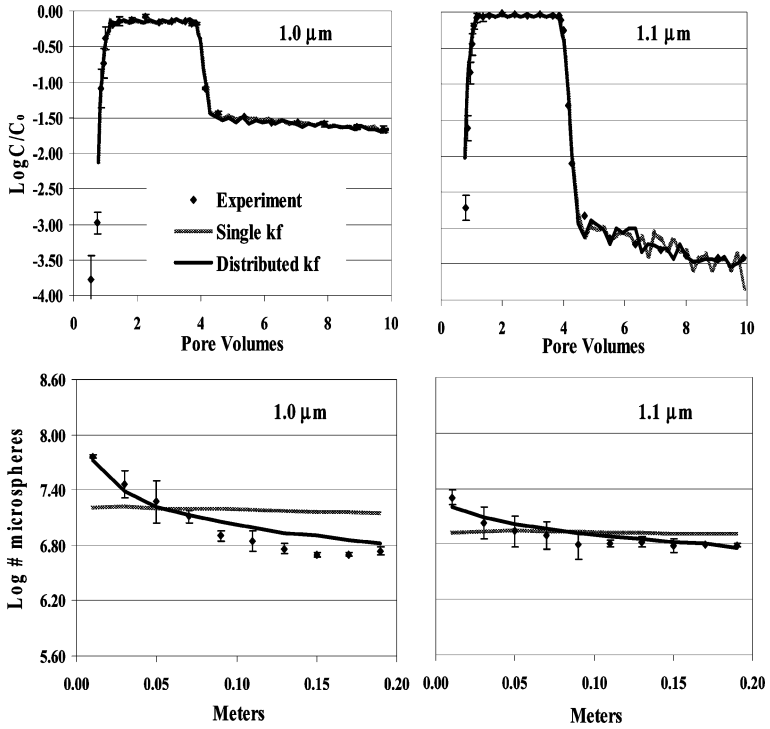

FIGURE 3. Comparison of the 1.0-μm and 1.1-μm microspheres at ionic strength = 0.02 M and flow rate = 8 m-day^{-1}, showing effluent breakthrough-elution curves (top) and retained profiles (bottom). Simulations are shown using the particle transport model with and without k_f distribution (solid and dashed line, respectively).

experiments (n=2). For all conditions (except 2 m-day^{-1} flow rate and 0.02M ionic strength) (Figure 2, top left), the breakthrough plateau (2−4 pore volumes) was constant, indicating a steady-state condition had been achieved. The exception showed continual decline in concentrations during breakthrough, indicating a temporal increase in the deposition rate coefficient during the course of injection (e.g. ripening). This experimental condition was simulated with a temporally constant deposition rate coefficient that reflected the average deposition rate coefficient during the experiment, since ripening was not a target process of this investigation.

The magnitude of the steady-state breakthrough plateau decreased with increasing ionic strength and decreasing flow rate (Figures 1 and 2, top). The breakthrough plateau for the 1.0-μm microspheres was lower, and tailing concentrations during elution were higher, relative to those for the 1.1 μm microspheres under an equivalent condition (8 m-day^{-1}, 0.02 M ionic strength) (Figure 3, top). The continuity of all breakthrough curves (Figures 1−3, top) indicates that minor flow interruption did not noticeably affect microsphere deposition and re-entrainment dynamics.

Inclusion of Retained Profile. At the lowest ionic strength (0.006 M), the normalized steady-state effluent plateau concentration was very close to unity (Figure 1, left top), which made the apparent fit of the steady-state plateau relatively insensitive to the value of the deposition rate coefficient. The retained microsphere profiles provided the information needed to further constrain the deposition rate coefficient, despite their comprising a minority of the overall mass at low ionic strength (Table 1). Although the effluent and retained concentrations were adjusted to yield 100% mass balance for the simulations, these adjustments were small as a result of the good mass balance and would not affect the analysis presented below. The magnitude of the retained microsphere profiles increased with increasing ionic strength and decreasing flow rate (Figures 1 and 2, bottom), in correspondence with the breakthrough curves.

Comparison of Fits with and without Deposition Rate Coefficient Distribution. The particle transport model was able to simulate well the effluent data regardless of whether a distribution in deposition rate coefficients was used (Figures 1−3, top). However, the retained profiles of microspheres could not be simulated using a constant rate coefficient of deposition. This was true for all experiments regardless of ionic strength, flow rate, and degree of carboxylation of the microspheres. In contrast, simulations using a distribution of deposition rate coefficients were capable of fitting well the retained profiles (Figures 1−3, bottom). Although regular trends were observed in the parameters derived from simulations (Table 1), most of these trends will be discussed in a separate paper that will examine the relationship of these trends to interaction forces and hydrodynamic drag. In the present paper, we will focus on trends that support explanations for the apparent decrease in the deposition rate coefficients with increased distance of transport.

Simulated Deposition Rate Coefficients and Distributions. Distributions of deposition rate coefficients used in the simulations varied predictably with ionic strength (Figure 4, left). The mean deposition rate coefficient increased with increasing ionic strength, while the standard deviation of the log-normal distribution ($\sigma_{\ln kf}$) showed the opposite trend, decreasing from 5.3 at 0.006 M to 1.8 at 0.05 M (Table 1, Figure 4, left). The probability of deposition for a given particle was equal to the product of its assigned deposition rate coefficient (h^{-1}) and the time step (h). Since our simulations utilized a time step of 0.01, any deposition rate coefficients equal to or greater than 100 h^{-1} resulted in deposition. Hence, deposition rate coefficients greater than 100 h^{-1} were set equal to 100 h^{-1} in the distributions shown. The low surface charge carboxylated microspheres (1.0 μm) showed greater $\sigma_{\ln kf}$ (3.2), than the high surface charge (1.1 μm) microspheres ($\sigma_{\ln kf}$ =2.3) under corresponding conditions (0.02 M ionic strength and 8 m-day^{-1} flow rate). These results demonstrate that distributions in deposition rate coefficient are governed at least in part by electrostatic interactions.

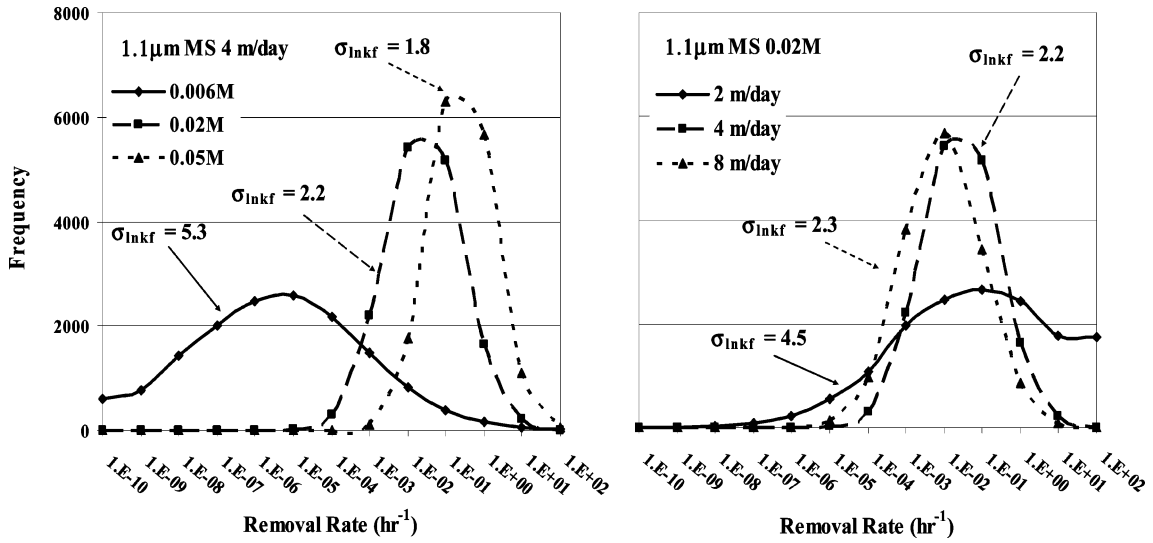

FIGURE 4. Distributions of deposition rate coefficients for the 1.1-μm microspheres (MS) versus ionic strength (left) and flow rate (right). Deposition rate coefficient values greater than 100 h^{-1} were set equal to 100 h^{-1} to reflect the unitary deposition probability for these rate coefficients under the 0.01 h time step used in the simulations.

The mean deposition rate coefficient decreased with increasing flow rate (Figure 4, right). However, the standard deviation (σ_{lnkf}) showed no clear trend in response to flow condition. Values of σ_{lnkf} first decreased dramatically from 4.5 at 2 m-day^{-1} to 2.2 at 4 m-day^{-1} and then slightly increased to 2.3 at 8 m-day^{-1}. The abrupt decrease in σ_{lnkf} from low to medium flow rate is most likely caused by ripening under this particular condition (Figure 2, left), which enhanced deposition at the inlet (*29*), adding extra steepness to the retained profile and requiring simulation using a much greater distribution of deposition rate coefficients. Hence, flow rate does not appear to significantly affect the distribution of deposition rate coefficients.

Discussion

Potential Artifacts Yielding Decreases in Deposition Rate Coefficient with Distance. It is possible that the apparent distributions in deposition rate coefficients reflect artifacts from the experimental set up. However, to explain the observed results, such an artifact would need to involve a change in some property between the influent and effluent ends of the column. Potential artifacts that must be considered for our experiments include variations with distance from the injection point of the glass bead packing or surface properties and changes in solution chemistry as well as the flow velocities as discussed below.

Sediment Heterogeneity. Sediment heterogeneity has been invoked as the origin of deposition rate coefficient decreases with increasing transport distances for viruses in at least one case where the column was purposefully made heterogeneous (*30*). In our case, enhanced deposition at the up-gradient end of the column could potentially be achieved if finer glass beads or fragments were mobilized toward the influent end of the column during equilibration, such that pore throat diameters at this end were effectively reduced. However, mobilization in this regard is unlikely, since mobilization of fine-grained glass fragments would likely result in their depletion from, rather than their concentration in, the influent end of the column. Stickier grain surfaces could potentially be generated at the influent end of the column during equilibration if geochemical processes occurred that were limited to (or exhausted within) that portion of the column. Grain surface alteration by the organic buffer MOPS might indeed occur due to adsorption of MOPS to the grain surfaces. However, as described below, decreases in deposition rate coefficients with distance were also observed in experiments lacking buffer, indicating that decreases in deposition rate coefficients were not caused by the MOPS buffer.

Changes in Solution Chemistry across the Column. Increases in pH across the column due to water-glass bead interaction could potentially increase repulsive interactions with down-gradient transport, thereby reducing the deposition rate coefficient with transport distance. However, pH of the effluent matched that of the influent and was constant throughout the experiments. Release of dissolved metals or metal oxides could potentially alter deposition rate coefficients with distance along the column. Qualitative measurements of the influent and effluent solutions using ICP-AES indicated no change in Na, Al, K, and Fe concentrations, whereas Si, Ca, and Mg concentrations increased by factors of about 2, 3, and 4, respectively, along the column. However, the measured conductivities of the influent and effluent solutions were equivalent within experimental error, due to the fact that the increases in Al, K, and Fe concentrations were above a negligible background (equivalent to purified water, Milli-Q). In addition, increases in metal ion concentrations would be expected to enhance rather than reduce the deposition rate coefficient. Finally, decreased deposition rate coefficient with distance was also observed in packed quartz sand buffered with $NaHCO_3$, a condition where metal releases and potential MOPS adsorption were absent (*31*).

Flow Heterogeneity. It is possible that spreading of flow across the diameter of the column upon entry into the column led to velocity variations (and presumably also variations in the deposition rate coefficient) at the influent end. To test this possibility, visible dye (food coloring) tracer tests were performed to examine the spreading of flow within the packed column. These tests clearly showed that the flow spread to the outer diameter of the column within 2 mm of the injection point, indicating that measures taken to spread flow evenly across the column were successful.

Generality of Apparent Decreases in Deposition Rate Coefficient with Distance. In the absence of an experimental artifact to cause the retained profiles to be steeper than predicted by theory, it appears that the steep profiles indicate a property of the system that deserves investigation. The nonexponential decrease of retained concentrations has been well observed in microbial transport and has been tentatively attributed to heterogeneity in cell surface properties among

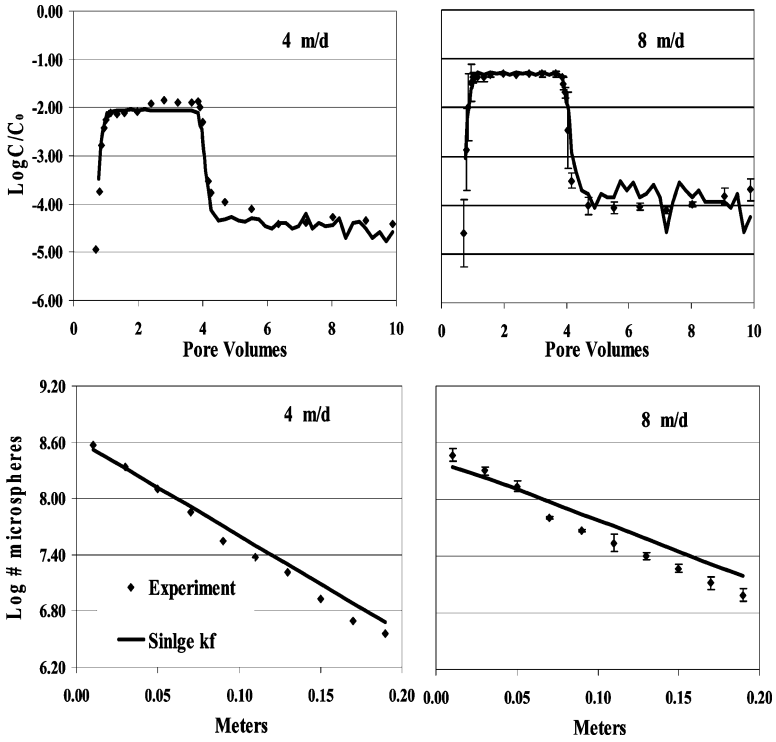

FIGURE 5. Effluent breakthrough-elution curves (top) and retained profiles (bottom) of amine-modified microspheres (0.93 μm) at flow rate = 4 m-day^{-1} (left) and 8 m-day^{-1} (right). Ionic strength = 0.001 M for both flow rates. The total injected number was normalized to the average total injected number of carboxylated microspheres (3.5 $\times$ 10^6 particle-mL^{-1}). In contrast to those of the carboxylated microspheres, effluent curves and retained profiles of the amine-modified microspheres could be simulated simultaneously using a single deposition rate coefficient.

the bacterial population (*1*, *3*−*6*). Surprisingly, very little attention has been focused on the retained profile in the literature concerning nonbiological colloid transport under clean bed conditions. The nonexponential profile observed here indicates that nonbiological particles such as microspheres also display apparent decreases in deposition rate coefficient with increased transport distance. Given the generality of this observation (where it has been investigated), its possible origins should be examined.

Conditions Promoting Apparent Decreases in Deposition Rate Coefficient. *Favorable Deposition and Mass Transport.* To determine possible boundaries on the experimental conditions under which apparent decreases in deposition rate coefficient would be observed, experiments were also run under electrostatically favorable conditions using positively charged microspheres (amine-modified polystyrene latex microspheres, 0.93 μm, Molecular Probes, Inc.). The influent concentration was 1.5 $\times$ 10^7 particles-mL^{-1}, and the experiments were run with MOPS buffer (0.001 M ionic strength, 4 and 8 m-day^{-1} flow rates). The breakthrough of the amine-modified microspheres was very low (Figure 5 top) due to the lack of an energy barrier to attachment. In contrast to those of carboxylated microspheres, the effluent breakthrough curves and retained profiles of amine-modified microspheres could be fit reasonably well simultaneously using a constant deposition rate coefficient (Figure 5), indicating that a spatially invariant deposition rate coefficient was relevant under favorable deposition conditions. The log-linear decrease in amine-modified microsphere concentration in sediment with distance (Figure 5, bottom) also argues against flow heterogeneity as a source of the decreases in deposition rate coefficients under unfavorable conditions, since it would manifest regardless of favorable or unfavorable conditions.

The experimental single deposition rate coefficients for amine-modified microspheres (derived via simulations) increased from 4.0 to 5.0 h^{-1} with an increase in flow rate from 4 to 8 m-day^{-1}. The magnitudes and trends of deposition rate coefficients can be compared with expectations from theory based on the following equation

$$k_f = \frac{3}{2}\frac{(1-\theta)}{d_c} v \alpha \eta \qquad (5)$$

where θ is porosity; v is the fluid velocity; and α is the collision efficiency, and d_c is the collector diameter. The value for the collision efficiency was set to unity to reflect favorable electrostatic conditions. The single collector efficiency, η, was calculated using the Rajagopalan-Tien model (*32*, *33*). The calculated k_f also increased with flow rate, from 6.5 h^{-1} at 4 m-day^{-1} to 8.1 h^{-1} at 8 m-day^{-1}, qualitatively in agreement with experimental values. Recently, Tufenkji and Elimelech. (*34*) refined the correlation equation to calculate the single collector efficiency by fully incorporating hydrodynamic interaction and van der Waals attractive forces. The deposition rate coefficients obtained using the TE equation (4.4 at 4 m-day^{-1} and 5.4 h^{-1} and 8 m-day^{-1}) match well the experimental values. Hence, the system behaved consistently with mass transport considerations under favorable deposition conditions.

Unfavorable Deposition and Mass Transport. Since retention in the up-gradient segments was somewhat reduced under unfavorable conditions relative to favorable conditions (Figures 1−3 and 5, bottom), the deposition rate coefficients under unfavorable conditions are also supported by mass transport considerations enveloped in filtration theory, even for the segments with the highest retention, thereby obviating the need to invoke filter ripening in order to produce the relatively high retained concentrations in the up-gradient segments under unfavorable conditions.

Deposition rate coefficients obtained from the TE equation and eq 5 (assuming α = 1) were compared to mean

experimental values obtained for the carboxylated microspheres (unfavorable conditions), to determine whether the mean values exceeded those supported by mass transport considerations. The theoretical maximum k_f for the 1.1-μm microspheres were 3.4, 4.0, and 4.9 h^{-1} at flow rates of 2, 4, and 8 m-day^{-1}, respectively. The theoretical maximum k_f for the 1.0-μm microspheres was 5.2 h^{-1} at 8 m-day^{-1}. The experimental mean k_f at each flow rate (Table 1) was less than or negligibly greater than the theoretical maximum k_f, except for 0.02 M at 2 m-day^{-1} for the 1.1-μm microspheres, where the experimental mean k_f (16.6 h^{-1}) greatly exceeded the theoretical maximum k_f (4.9 h^{-1}). Under this particular condition significant filter ripening occurred (Figure 2, left), which presumably enhanced the experimental deposition rate coefficient. That the experimental mean deposition rate coefficients did not significantly exceed the theoretical maximum deposition rate coefficients indicates that mass transport considerations permit the existence of log-normally distributed deposition rate coefficients. The maximum deposition rate coefficent in the simulated distributions was 100 h^{-1}. At first glance this maximum deposition rate coefficient appears to violate mass transport considerations; however, it must be recalled that this value represents individual microspheres, whereas the deposition rate coefficient obtained from filtration theory represents an average for the system.

Origin of Apparent Decreases in Deposition Rate Coefficient with Transport Distance. In determining the origin of spatially variable colloid deposition rates across a packed sand column, the significance of the steady-state effluent plateau must be emphasized, since it indicates that the overall deposition rate across the column is temporally constant, whereas spatially, the deposition is relatively enhanced in the up-gradient end of the column (or relatively depleted in the down-gradient end). The temporal constancy of the deposition rate appears to further disqualify filter ripening at the up-gradient end of the column as an origin, since tying the deposition rate coefficient to the retained concentration would likely result in a temporally increasing deposition rate coefficient and declining breakthrough plateau. Given these constraints, potential origins include the following: (1) distributed deposition rate coefficients (interaction potentials) among the colloidal population; (2) straining at the influent end of the column; and (3) depletion of colloid concentrations in the perimeter of the pores adjacent to the grain surfaces due to deposition from solution.

Distributed Interaction Potentials among the Colloid Population. The preferential deposition of a fraction of the colloid population at the influent end of the column could potentially result from a distribution of interaction potentials among that population, a mechanism that has been well invoked in the microbial transport literature. It is not clear whether such a mechanism is applicable to nonbiological colloids. The standard deviations of the deposition rate coefficients determined from simulation of our system under unfavorable conditions range between 1.8 and 5.3 (on natural log scale), with the largest values corresponding to the lowest ionic strength for the 1.1-μm microspheres at 4 m-day^{-1}. Their corresponding range in log scale is from less than 1 to about 2. This range, over 1−2 orders of magnitude, is much greater than that previously considered for distributed interaction potentials in the nonbiological colloid transport literature (*17*). However, a relatively mild range in interaction energies may generate a large range in deposition rate coefficients, since the deposition rate coefficient is exceedingly sensitive to the interaction potential (*25*), as shown in the expression below from Ryan and Elimelech (*35*), which is based on the work of Ruckenstein and Prieve (*36*) and Dahneke (*37*)

$$k_f \propto \exp\left(-\frac{\phi_{\max}}{kT}\right) \tag{6}$$

where k is the Boltzmann constant, T is the temperature, and $\phi_{\max}$ is the maximum interaction potential corresponding to the energy barrier.

Since the largest modeled standard deviation of k_f (in natural log space) was 5.3

$$\ln k_f = \ln k_{f(mean)} \pm 5.3 \tag{7}$$

Then

$$\frac{\phi_{\max}}{kT} = \frac{\phi_{\max\,(mean)}}{kT} \pm 5.3 \tag{8}$$

Therefore

$$\phi_{\max} = \phi_{\max\,(mean)} \pm 5.3kT \tag{9}$$

The above equation indicates that a variation in the interaction potentials of about 5.3 kT can explain 2 orders of magnitude distribution in deposition rate coefficient observed here. Variation of 5.3 kT is a factor of 3.5 greater than the 1.5 kT energy intrinsic to all colloids, molecules, etc. Such a variation in the interaction energy can be caused, for example, by minor variations in the surface potentials developed from measured electrophoretic mobilities (EPM). To yield a 5.3 kT variation, the surface potentials determined for the microspheres would need to show variations of about 0.5% or less (*38*), e.g. −40.0 mV versus −39.8 mV (0.006 M, Hamaker constant = 3.8×10^{-21} J), a variation that would likely be undetectable in our EPM measurements. In fact, by deconvoluting the experimental EPM distribution to eliminate the contribution from random Brownian diffusion, Dong (*39*) recently found the EPM distribution for 300 nm latex carboxylated polystyrene latex microspheres ranged over 3 units (10^{-8} m^2 V^{-1} s^{-1}), a distribution that would yield a variation far greater than 0.5% of any expected surface potential value (typically <−100 mV). Although eq 6 assumes that deposition occurs in the primary minimum, distributed properties may just as well govern retention in the secondary minimum, e.g. distribution in secondary minimum depth. The Maxwell distribution of intrinsic energies may also govern the ability of colloids to escape the secondary minimum (*40*).

Straining. Bradford et al. (*23*) observed that retained profiles of carboxylated microspheres following transport experiments in glass beads and quartz sands were not consistent with a constant deposition rate coefficient. Furthermore, deposition was favored by larger colloid size despite the prediction from filtration theory that collector efficiencies would be lowest for the 2 μm relative to the other sizes of microspheres examined (0.45, 1.0, and 3.2 μm). The authors therefore concluded that physical straining caused enhanced deposition of microspheres at the influent end of the columns.

The hypothesis that straining enhances deposition at the influent end of the column is intriguing and deserves further study, since, as stated by Bradford et al. (*23*), entrapment of colloids in "dead-end" pores can be reasonably expected to occur during movement of the colloid suspension from the surface (where fluid flow is evenly distributed across the pore domain) to the interior (where fluid flow is constrained to continuous pores). However, the sensitivity of the retained profile to ionic strength demonstrated here precludes purely

physical straining as the primary mechanism of generating decreases in deposition rate coefficient with distance of transport.

It is possible that colloid aggregation plays a role in straining. For example, our flow cytometry results show that the influent solutions included 1.5% doublets and <0.3% triplets for the 1.1-μm microspheres and less than 1.0% doublets and negligible triplets for the l.0-μm microspheres, consistent with the manufacturer's claim. These values were the same regardless of ionic strength, indicating that the presence of doublets and triplets may represent a manufacturing artifact rather than aggregation. The effluent samples for the 1.1-μm microspheres showed 1.2% doublets and <0.15% triplets, indicating a decrease in the frequency of these "aggregates" in the mobile phase during transport. The percentage of doublets of the 1.0-μm microspheres in the effluent displayed no noticeable difference from that in the influent. For the 1.1-μm microspheres at the low ionic strength (0.006 M), the number of doublets and triplets in the influent was a significant fraction of the number of retained microspheres (about 60%); therefore, straining of doublets and triplets could be potentially a significant (even dominant) contributor to microsphere retention at low ionic strengths. Thus straining may explain the abrupt decrease in $\sigma_{\ln kf}$ from 0.006 M (5.3) to 0.02 M (2.2). At higher ionic strengths, however, the numbers of doublets and triplets for both microspheres in the influent were negligible relative to the number of retained microspheres, and so straining of doublets and triplets was at most a relatively minor contributor to decrease in deposition rate coefficient with transport distance at the higher ionic strengths. As indicated in Bradford et al. (*23*), straining has traditionally been considered insignificant when the diameter ratio of colloid to grain is less than 0.05 (*41*, *42*), a value far greater than the ratio in this study (approximately 0.002).

Depletion of Aqueous Particle Concentration at Pore Perimeter. Depletion of colloids from the pore water adjacent to grain surfaces by deposition to grain surfaces is an additional possible mechanism that might generate the apparent decreases in deposition rate coefficient with distance of transport. Existing colloid filtration theory does not distinguish colloid concentrations in the pore perimeter from colloid concentrations in the bulk pore water; however, depletion of colloids in the pore perimeter is a reasonable expectation if deposition of colloids at the pore perimeter exceeds replenishment of colloids by diffusion and settling across flow lines. Rapid depletion of colloids in the pore perimeter could therefore explain the steep high concentration portion of the retained colloid profile proximal to the injection point, whereas replenishment of colloids to the pore perimeter might explain the relatively low concentration flat portion of the retained colloid profile distal to the injection point. However, the observed log-linear decrease in the number of retained amine-modified microspheres (Figure 5, bottom) precludes such an explanation, since depletion of colloids in the pore perimeter would also manifest under favorable conditions.

Implication. The generality of apparent decreases in deposition rate coefficient with increased transport distance among nonbiological and biological colloids indicates control by processes that are fundamental to filtration under unfavorable conditions. Although straining may be a significant contributor to decreases in deposition rate coefficient with increasing transport distance at low ionic strength, it is a minor contributor at high ionic strength where much greater overall retention is observed. Distributions in interaction potentials remain a viable contributor to decreases in colloid deposition rate coefficients with increasing transport distance.

Acknowledgments

This work was funded by a grant from the National Science Foundation Hydrologic Sciences Program (EAR 0087522) to W. P. Johnson. The authors wish to thank Dr. Saskia Duyvesteyn at Department of Metallurgical Engineering of University of Utah for her help with the ICP-AES measurements. W.P.J. also wishes to thank Dr. Charles O'Melia at The Johns Hopkins University for many helpful discussions that contributed to improvement of this manuscript. Any opinions, findings, and conclusions or recommendations expressed in this material are those of the authors and do not necessarily reflect the views of the National Science Foundation.

Literature Cited

(1) Albinger, O.; Biesemeyer,B. K.; Arnold, R. G.; Logan, B. E. *FEMS Microbiol. Lett*. **1994**, *124*, 321−326.
(2) Yao, K.; Habibian, M. T.; O'Melia, C. R. *Environ. Sci. Technol*. **1971**, *5* (11), 1105−1112.
(3) Baygents, J. C.; Glynn, J. R., Jr.; Albinger, O.; Biesemeyer, B. K.; Ogden, K. L.; Arnold, R. G. *Environ. Sci. Technol*. **1998**, *32*, 1596−1603.
(4) Simoni, S. F.; Harms, H.; Bosma, T. N. P.; Zehnder, A. J. B. *Environ. Sci. Technol*. **1998**, *32*, 2100−2105.
(5) Bolster, C. H.; Mills, A. L.; Hornberger, G.; Herman, J. *Water Resour. Res*. **1999**, *35*, 1797−1807.
(6) Bolster, C. H.; Mills, A. L.; Hornberger, G.; Herman, J. *Ground Water* **2000**, *38*, 370−375.
(7) Harvey, R. W.; Garabedian, S. P. *Environ. Sci. Technol*. **1991**, *25*, 178−185.
(8) Deflaun, M. F.; Murray, C. J.; Holben, M.; Scheibe, T.; Mills, A.; Ginn, T.; Griffin, T.; Majer, E.; Wilson, J. L. *FEMS Microbiol. Rev*. **1997**, *20*, 473−487.
(9) Zhang, P.; Johnson, W. P.; Scheibe, T. D.; Choi, K.-H.; Dobbs, F. C.; Mailloux, B. J. *Water Resour. Res*. **2001**, *37* (11), 2687−2698.
(10) Redman, J. A.; Grant, S. B.; Olson, T. M.; Estes, M. K. *Environ. Sci. Technol*. **2001**, *35* (9), 1798−1805.
(11) Redman, J. A.; Estes, M. K.; Grant, S. B. *Coll., Surf. A: Physicochem. Eng. Asp*. **2001**, *191*, 57−70.
(12) Bales, R. C.; Li, S. M.; Yeh, T. C. J.; Lenczewski, M. E.; Gerba, C. P. *Water Resour. Res*. **1997**, *33*, 639−648.
(13) Pieper, A. P.; Ryan, J. N.; Harvey, R. W.; Amy, G. L.; Illangasekare, T. H.; Metge, D. W. *Environ. Sci. Technol*. **1997**, *31*, 1163−1170.
(14) Schijven, J. F.; Hoogenboezem, W.; Hassanizadeh, S. M.; Peters, J. H. *Water Resour. Res*. **1999**, *35* (4), 1101−1111.
(15) Woessner, W. W.; Ball, P. N.; DeBorde, D. C.; Troy, T. L. *Ground Water* **2001**, *36* (6), 886−894.
(16) Tufenkji, N. J.; Redman, J. A.; Elimelech, M. *Environ. Sci. Technol*. **2003**, *37*, 616−623.
(17) Elimelech, M.; O'Melia, C. R. *Langmuir* **1990**, *6* (6), 1153−1163.
(18) Kallay N.; M. T.; Biškup, B.; Kunjašic, I.; Matejević, E. *Coll., Surf*. **1987**, *28*, 185−187.
(19) Barouch, E.; Wright, T. H.; Matejević, E.; *J. Coll. Int. Sci*. **1987**, *118* (2), 473−481.
(20) Weiss, M.; Luthi, Y.; Rička, J. *J. Coll. Int. Sci*. **1998**, *206*, 322−331.
(21) Grolimund, D. K.; Borkovec, M. *Environ. Sci. Technol*. **1999**, *33* (2), 4054−4060.
(22) Grolimund D.; Barmettler, K.; Borkovec, M. *Water Resour. Res*. **2001**, *37* (3), 571−582.
(23) Bradford. S. A.; Yates, S. R.; Bettahar, M.; Simunek, J. *Water Resour. Res*. **2002**, *38* (12), 1327−1338.
(24) Litton, G. M.; Olson, T. M. *Environ. Sci. Technol*. **1993**, *27*, 185−193.
(25) Elimelech, M.; O'Melia, C. R. *Environ. Sci. Technol*. **1990**, *24* (10), 1528−1536.
(26) Scheibe, T. D.; Wood, B. D. *Water Resour. Res*. **2003**, *39* (4), doi: 10.1029/2001WR001223.
(27) Toride, N.; Leij, F. J.; van Genuchten, M. T. U.S. Salinity Lab, Agric. Res. Serv., Riverside, CA, 1995, Res. Report 137.
(28) Soong, T. T. *Probabilistic Modeling and Analysis in Science and Engineering*; John Wiley and Sons: 1981, 384pp.
(29) O'Melia, C. R.; Ali, W. *Prog. Water Technol*. **1978**, *10* (5−6), 167−182.
(30) Li, X.; Johnson, W. P. **2004**, submitted.
(31) Schijven, J. F.; Hassanizadeh, S. M.; de Bruin H. A. M. *J. Contam. Hydrol*. **2002**, *58*, 243−259.

(32) Rajagopalan, R.; Tien, C. *AIChE* **1976**, *22* (3), 523−533.
(33) Logan, B. E.; Jewett, D. G.; Arnold, R. G.; Bouwer, E. J.; O'Melia, C. R. *J. Environ. Eng.* **1995**, 869−873.
(34) Tufenkji, N.; Elimelech, M. *Environ. Sci. Technol.* **2004**, *38*, 529−536.
(35) Ryan, J. N.; Elimelech, M. *Coll., Surf. A: Physicochem. Eng. Asp.* **1996**, *107*, 1−56.
(36) Ruckenstein, E.; Prieve, D. C. *AIChE J.* **1976**, *22*, 276.
(37) Dahneke, B. *J. Colloid Interface Sci.* **1975**, *50*, 194.
(38) Assemi, S.; Johnson, W. P.; Li, X. **2004**, in preparation.
(39) Dong, H. *J. Microbiological Methods* **2002**, *51*, 83−93.
(40) Hahn, M. W.; O'Melia, C. R. *Environ. Sci. Technol.* **2004**, *38*, 210−220.
(41) Sakthivadivel, R. Hydraulic Engineering Laboratory, University of California, Berkeley, 1966, HEL15-5.
(42) Sakthivadivel, R. Hydraulic Engineering Laboratory, University of California, Berkeley, 1969, HEL15-7.

Received for review June 5, 2004. Revised manuscript received August 19, 2004. Accepted August 19, 2004.

ES049154V